FOAMS® 2021

September 13-16, 2021 • Virtual Conference

Presented by SPE Thermoplastic Materials & Foams Division

Conference Proceedings

Fabrication and characterization of low-density nanocellular foam based on PMMA/TPU blends

Nigus Maregu Demewoz and Shu-Kai Yeh

Department of Materials Science and Engineering, National Taiwan University of Science and Technology, Taipei, Taiwan, Republic of China

Abstract

In nanocellular foam production, achieving cell sizes less than 100 nm with relative densities less than 0.25 is challenging. In this study, PMMA was blended with three different hardnesses of thermoplastic polyurethanes (TPU) to study their effects on the cellular structure. The TPU was well dispersed in the PMMA matrix with a domain size of less than 300 nm. The PMMA/TPU blends were foamed with a two-step foaming process using CO_2 as the blowing agent. The results show that the hardness and viscosity of TPU controlled the nanostructure of the blend and affected the foam morphology. The TPU with high hardness and viscosity produced the smallest domain size and the highest cell density, resulting in a low relative density. This is the first report of a special bouquet nanocellular structure with an average cell size of less than 100 nm and a relative density of less than 0.2.

Keywords: Nanocellular foam, PMMA-TPU blend, domain size, low-density, open-cell,

1. Introduction

Polymer foam materials have many excellent properties, such as their light weight and their thermal insulation, sound insulation, and cushioning properties. Because of these applications, the recent advancements in nanocellular foam have attracted significant interest in academia. Interest has risen in thermal insulation applications because the thermal insulation system maintains ambient heat energy and minimizes CO_2 emission [1-3]. The gas conduction in nanocellular foams with a cell size of less than 100 nm is significantly reduced due to the Knudsen effect [4].

For the production of nanocellular foam, solid-state foaming technology has been proven in the laboratory to be economical and viable. Also, Costeux et al. [2] summarized the use of polymers for making CO_2-blown nanocellular polymer foams. PMMA is the most common polymer used for this process because the carbonyl groups in PMMA, which have a high affinity with CO_2 and high CO_2 solubility, are essential [5].

Adding elastomers as a nucleating agent decreases the cell size and increases cell density. Ramesh et al. [6] studied the nucleation effect of rubber particles using N_2 as the blowing agent. They compounded HIPS with polystyrene (PS) to get 0.03, 0.3, and 3% rubber in PS and see the impact of nucleating agent concentration on PS foam. They found that the cell density is in proportion to the particle size at 1% HIPS loading. If the particle size is less than 300 nm, it may affect the cell density. On the other hand, the blend of polypropylene (PP) with thermoplastic polyolefin (TPO) shows that the size of the dispersed elastomer affects the cell structure [7] .

Poly (methyl methacrylate)–poly (butyl acrylate)–poly (methyl methacrylate) (MAM) generates a nanocellular structure and reduces relative density [8-11]. The MAM has a high CO_2 affinity. In these studies, researchers achieved a nanocellular foam with the lowest relative density, about 0.23, and a cell size of 350 nm. In addition to MAM, TPU has been used as a nucleating agent to lower the relative density and to increase the toughness of the nanocellular foam [11]. In another example, adding TPU created a gradient foam structure [12]. In addition, adding TPU to PMMA may lower the relative density to 0.125 with an average size of 205 nm [11].

This study examines the effects of the hardness and the particle size of TPU. By adding 2 wt% of TPU, we produced a nanocellular material with an average cell size of less than 100 nm with a relative density of 0.18 to 0.28.

2. Experimental Section

2.1 Materials

PMMA of molecular weight 82,400 g/mol was purchased from ChiMei Corporation. The blowing agent, carbon dioxide (CO_2) of 99.9% purity, was purchased from Wanan Gas Corporation. For this study, three different hardnesses of polyether-based TPUs were supplied by Kin Join Co., Ltd. The details are shown in Table 1.

PMMA and 2 wt% of TPU were compounded using the Xplore MC-15 twin-screw micro compounder at 210 °C with a screw speed of 60 rpm for 5 minutes. Based on the TPU hardness content, we named our blends as follows: the combination of PMMA with E-385A, E-390A, and E-395A are called PMMA-TPU385, PMMA-TPU390, and PMMA-TPU395, respectively. A two-step foaming method was applied to foam the PMMA-TPU blend. The PMMA-TPU samples were saturated at 13.79 MPa and 0 °C for 12 hours and foamed at 70 °C for 3 minutes.

Each compounded sample was immersed in tetrahydrofuran (THF) solvent to selectively dissolve the TPU particles from the matrix [18]. The etched morphology and the foam structure of the blend were observed using an FEI Quanta 3D FEG dual beam Focused Ion Beam (FIB). The SEM pictures were analyzed with Image J software. The cell density was calculated using the following equation:

$$N_0 = \left(\frac{nM^2}{A}\right)^{\frac{3}{2}}\left(\frac{\rho_s}{\rho_f}\right) \quad (1)$$

where N_0 is the cell density (cells/cm^3), n is the number of cells, M is the magnification, A is the area of the picture (cm^2), ρ_s is the density of the solid sample (g/cm^3), and ρ_f is the density of the foamed sample (g/cm^3).

The solubility of CO_2 can be determined by the mass loss analysis method. To determine the CO_2 solubility by the mass loss method, we plotted the mass loss versus the square root of time and extrapolated the curve linearly to the zero-desorption time [13-15].

3. Results and Discussion

3.1 Phase Morphology of PMMA-TPU Blends

The chemical-etched PMMA-TPU blend phase morphology was characterized using SEM images [7, 12]. Figure 1 shows the phase morphology of the PMMA-TPU blend after etching while Figure 2 shows the TPU particle size distribution and density. After etching, pores of several hundred nanometers are dispersed in the PMMA matrix. The size of the area left when the particles are dissolved by THF during etching is considered the size of the particles.

The phase morphology of the PMMA-TPU blends changes with the hardness [7]. Interestingly, the dispersed phase particle size decreases with the increase in TPU hardness. The average particle sizes were 0.289 μm, 0.250 μm, and 0.088 μm for PMMA-TPU385, PMMA-TPU390, and PMMA-TPU395. The frequency distributions of TPU particle sizes in PMMA, which are shown in Figure 1 (a), clearly demonstrate that PMMA-TPU395 presents a narrow size distribution as compared with PMMA-TPU385 and PMMA-TPU390, a difference that may significantly affect the nucleation efficiency. Similar phenomena have been reported in nanosilica nucleating agents [16-19].

Figure 2(b) shows the density of TPU particles. The particle density of the PMMA-TPU395 blend shows one order of magnitude higher than that of the PMMA-TPU385 and PMMA-TPU390 blends. The smaller dispersed particles increase the particle density, which results in the total number of heterogeneous nucleation sites. The viscosity ratio of the blends manipulates the TPU particle size, as shown in Table 2. The calculated particle size was consistent with the experimental values obtained from the SEM images (Table 2). Because of its high particle density, PMMA-TPU395 shows the smallest interparticle distance.

3.2. The effects of TPU Hardness on PMMA-TPU Foam

The PMMA and PMMA/TPU blends saturated at 13.78 MPa and 0 ºC for 12 hours and foamed at 70 ºC for 3 minutes were characterized to evaluate the effects of different TPU hardness on the cell structure. The CO_2 solubility of the blends and the foam structural parameters are summarized in Table 3. Because TPU usually absorbs less CO_2 than PMMA [12] and because the soft segments tend to absorb more CO_2 [20], the CO_2 solubility of the blends decreased with TPU hardness. Nevertheless, the decrease did not affect the generation of the nanocellular structure. Guo et al. reported that the critical CO_2 solubility for generating PMMA nanocellular foam is 30.1 - 32.6 wt% [5]. The CO_2 solubility value of the blends in this study is well above that value.

Figure 3 shows the foam morphology of the pure PMMA and the PMMA-TPU blends. The first and second rows of SEM pictures in Figure 3 shows the macroscopic structure of the foam. The cells are fine and uniform. However, the high magnification SEM pictures in the third and fourth rows show the sub-micron and nanocellular structure.

Pure PMMA shows more solid-like and homogenous cells as compared to the PMMA-TPU blend. The ratio between the standard deviation and the average cell size (SD/ϕ) measures the homogeneity of foam structures [21]. The SD/ϕ value of PMMA is lower than 0.04, implying good homogeneity, while in the PMMA/TPU blend, the SD/ϕ value is more than 0.5, showing the heterogeneity of the cellular structure. The PMMA-TPU blend shows a bouquet-like system consisting of nanocellular cells and some sub-micron cells. In addition, the TPU particles can be seen in the center of the sub-micron cells. We believe it is evidence of TPU particles acting as nucleation agents.

The cell density of the PMMA-TPU blend is much higher than 1.6×10^{15} cells/cm^3, which is the cell density of neat PMMA. Also, the cell density is 1000~3500 times higher than the particle density. Costeux et al. estimated the nucleation efficiency by dividing the cell density by the particle density with the assumption of one particle nucleate, one cell [22]. Liu et al. used silica nanoparticles as a heterogeneous nucleation agent and found a less-than-six-fold

nucleation efficiency [23]. Our results show that the nucleation efficiency could be much higher than 100%; therefore, their assumptions might have overlooked some facts. The cell densities of these three blends are similar. The results imply that high particle density does not significantly increase cell density. There are two possible reasons. First, the CO_2 solubility of PMMA/TPU 385 is the highest among the blends. High solubility led to a high nucleation rate and potentially high cell density. Secondly, although the inter-particle distance increased with decreasing particle density, homogenous nucleation happened even in the absence of a nucleating agent [24]. Also, we suspect that homogeneous nucleation or spinodal decomposition may happen in between the nucleuses [25]. For these reasons, the cell density did not drop significantly.

As shown in Table 2, the relative density of PMMA-TPU foam is lower than that of the neat PMMA foam. Compared with neat PMMA foam, adding 2 wt% TPU to PMMA reduces the relative density by at least another 18-20%. Among the blends, PMMA-TPU395 presents the lowest relative density, 0.22. Because the average cell size didn't change significantly, such a reduction is caused by increased cell density. Moreover, the decrease in the strut fraction helps reduce the relative density of nanocellular foam [26]. At the moment, the lowest density of nanocellular foam available with a cell size less than 100 nm is about 0.21 [22]. Nevertheless, Liu et al. did not remove the microcellular transition layer. Removing the transition layer, in general, causes an increase in density because it is composed of micro-sized cells. The transition layer becomes thicker with increasing desorption time, resulting in a decrease in density [25, 27].

Conclusions

Low-density nanocellular foam has been produced through a two-step foaming process. PMMA was melt-blended with TPU of different hardnesses using a twin-screw micro-compounder. Because of the nanometric TPU particle dispersion in the PMMA matrix, the solid PMMA-TPU blend presents a nanostructure. The morphology, particle size, and particle density of the nanostructure varied with the TPU hardness. We observed a very particular bouquet-like bimodal structure consisting of nanocellular and sub-micron cells. The PMMA-TPU blend produces low-density nanocellular foam. The smaller particle size PMMA-TPU395 generates a lower average cell size and higher cell density resulting in lower relative density. With an average cell size of less than 100 nm, we produced a relative density of less than 0.2.

Table 1: Ether-based TPU of different grades

Commercial name of TPU	Sample Name	Hardness (Shore A)	Density (g/cm^3)	Hard segment content (wt%)	MFI (g/ 10 min)
E-385A	TPU385	85	1.12	39.3	18.5
E-390A	TPU390	90	1.12	45.9	16.7
E-395A	TPU395	95	1.13	50.4	23.5

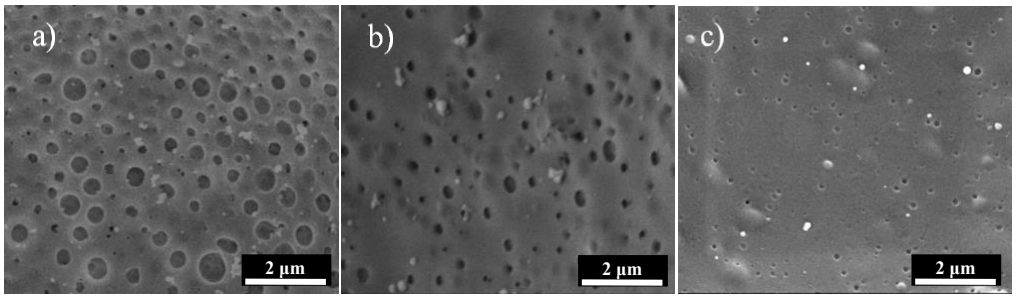

Figure 1 The phase morphology of PMMA-TPU after etching with THF (a) PMMA-TPU385 (b) PMMA-TPU390 and (c) PMMA-TPU395

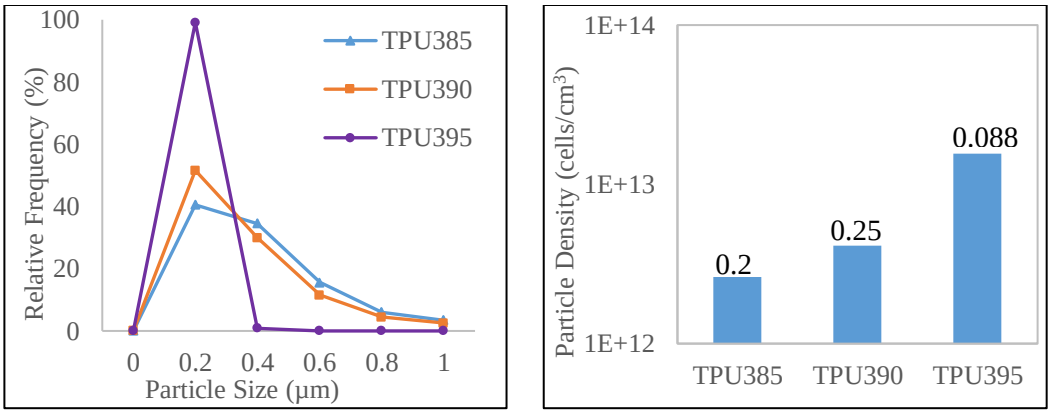

(a) (b)

Figure 2 (a) Particle size distribution and (b) Particle size with a particle density of PMMA-TPU

Table 2 The capillary number, viscosity ratio, theoretical and experimental values for minimum particle size, and inter-particle distance of the blend.

Blend	Viscosity Ratio (p)	Theoretical estimation of minimum particle diameter (nm)	The experimental value of minimum particle diameter (nm)	Interparticle distance (nm)
PMMA-TPU385	0.0026	135	93	520
PMMA-TPU390	0.0052	74	63	290
PMMA-TPU395	0.0074	53	48	210

Table 3 CO_2 solubility, relative density (RD), average cell size, cell density, SD/$\boldsymbol{\phi}$, and open-cell content of PMMA and PMMA-TPU foamed at 70 °C

Sample	CO_2 solubility (wt%)	RD Before skin layer removal	RD After skin layer removal	Average cell size (nm)	SD/$\boldsymbol{\phi}$	Cell Density (nuclei/cm^3)
PMMA	38.14	0.28	0.31	55	0.04	1.60×10^{15}
PMMA-TPU385	37.30	0.24	0.25	65	0.59	9.60×10^{15}
PMMA-TPU390	36.36	0.24	0.25	57	0.68	1.48×10^{16}
PMMA-TPU395	34.95	0.22	0.22	44	0.61	1.82×10^{16}

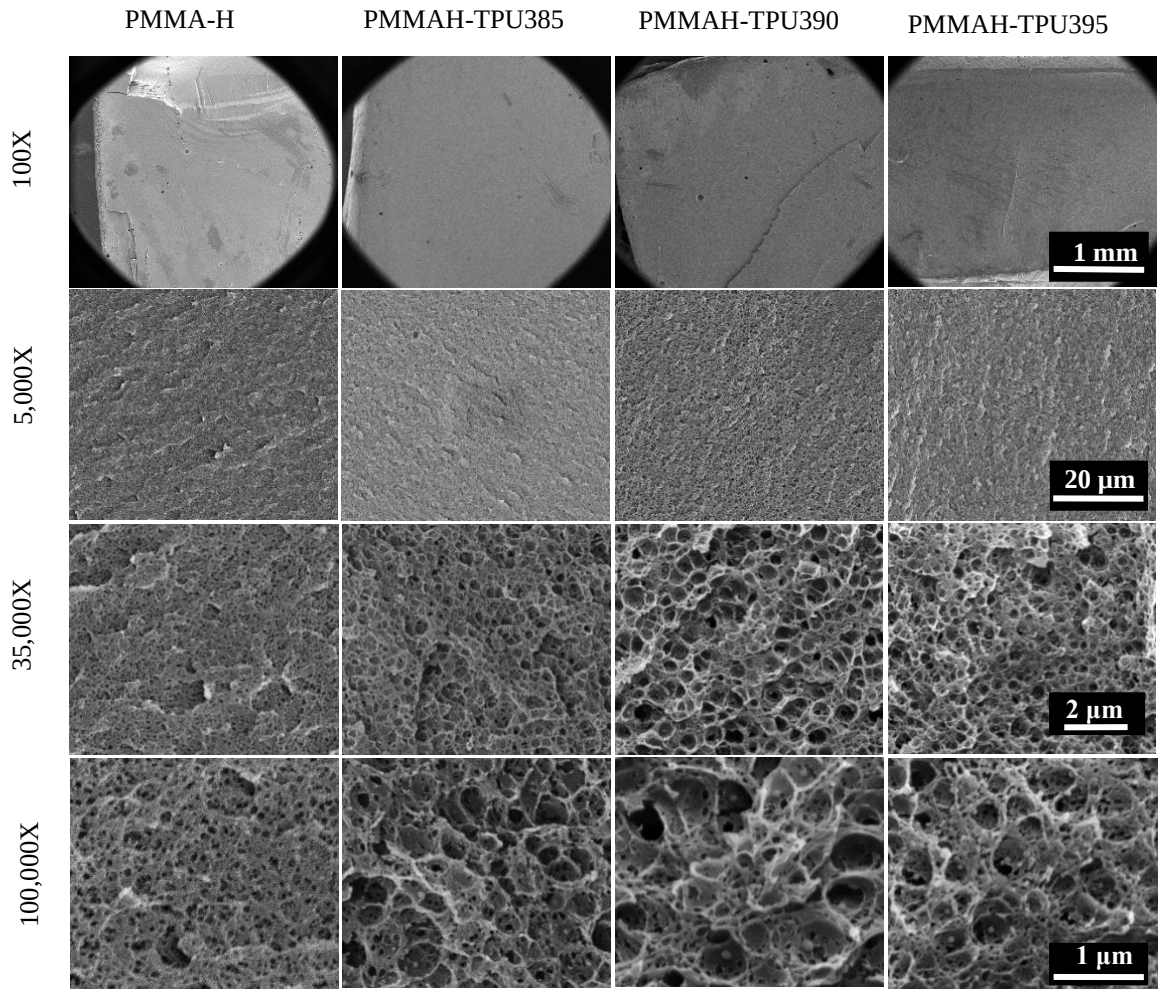

Figure 3 The morphology of PMMA-TPU blends at T_f = 70 °C

References

1. Notario, B., J. Pinto, and M.A. Rodriguez-Perez, Nanoporous polymeric materials: A new class of materials with enhanced properties. Progress in Materials Science, 2016. **78-79**: p. 93-139.
2. Costeux, S., CO2-blown nanocellular foams. Journal of Applied Polymer Science, 2014. **131**(23).
3. Wang, G., et al., Low-density and structure-tunable microcellular PMMA foams with improved thermal-insulation and compressive mechanical properties. European Polymer Journal, 2017. **95**: p. 382-393.
4. Notario, B., et al., Experimental validation of the Knudsen effect in nanocellular polymeric foams. Polymer, 2015. **56**: p. 57-67.
5. Guo, H., A. Nicolae, and V. Kumar, Solid-state poly(methyl methacrylate) (PMMA) nanofoams. Part II: Low-temperature solid-state process space using CO2 and the resulting morphologies. Polymer, 2015. **70**: p. 231-241.
6. Ramesh, N.S., D.H. Rasmussen, and G.A. Campbell, The heterogeneous nucleation of microcellular foams assisted by the survival of microvoids in polymers containing low glass transition particles. Part II: Experimental results and discussion. Polymer Engineering & Science, 1994. **34**(22): p. 1698-1706.
7. Kim, S.G., et al., The effect of dispersed elastomer particle size on heterogeneous nucleation of TPO with N_2 foaming.

Chemical Engineering Science, 2011. **66**(16): p. 3675-3686.
8. Forest, C., et al., Nanofoaming of PMMA using a batch CO2 process: Influence of the PMMA viscoelastic behaviour. Polymer, 2015. **77**: p. 1-9.
9. Bernardo, V., et al., Understanding the role of MAM molecular weight in the production of PMMA/MAM nanocellular polymers. Polymer, 2018. **153**: p. 262-270.
10. Bernardo, V., et al., Low-density PMMA/MAM nanocellular polymers using low MAM contents: Production and characterization. Polymer, 2019. **163**: p. 115-124.
11. Wang, G., et al., Ultra-tough and super thermal-insulation nanocellular PMMA/TPU. Chemical Engineering Journal, 2017. **325**: p. 632-646.
12. Bernardo, V., et al., Nanocellular Polymers with a Gradient Cellular Structure Based on Poly(methyl methacrylate)/Thermoplastic Polyurethane Blends Produced by Gas Dissolution Foaming. Macromolecular Materials and Engineering, 2020. **305**(1): p. 1900428.
13. Pantoula, M. and C. Panayiotou, Sorption and swelling in glassy polymer/carbon dioxide systems: Part I. Sorption. The Journal of Supercritical Fluids, 2006. **37**(2): p. 254-262.
14. Guo, H. and V. Kumar, Some thermodynamic and kinetic low-temperature properties of the PC-CO2 system and morphological characteristics of solid-state PC nanofoams produced with liquid CO2. Polymer, 2015. **56**: p. 46-56.
15. Yeh, S.-K., N.M. Demewoz, and V. Kurniawan, Controlling the structure and density of PMMA bimodal nanocellular foam by blending different molecular weights. Polymer Testing, 2021. **93**: p. 107004.
16. Famili, M.H.N., H. Janani, and M.S. Enayati, Foaming of a polymer-nanoparticle system: Effect of the particle properties. Journal of Applied Polymer Science, 2011. **119**(5): p. 2847-2856.
17. Janani, H. and M.H.N. Famili, Investigation of a strategy for well controlled inducement of microcellular and nanocellular morphologies in polymers. Polymer Engineering & Science, 2010. **50**(8): p. 1558-1570.
18. Zakiyan, S.E., M.H.N. Famili, and M. Ako, Controlling foam morphology of polystyrene via surface chemistry, size and concentration of nanosilica particles. Journal of Materials Science, 2014. **49**(18): p. 6225-6239.
19. Goren, K., et al., Influence of nanoparticle surface chemistry and size on supercritical carbon dioxide processed nanocomposite foam morphology. Journal of Supercritical Fluids, 2010. **51**(3): p. 420-427.
20. Ito, S., et al., Generation of microcellular polyurethane with supercritical carbon dioxide. Journal of Applied Polymer Science, 2007. **106**(6): p. 3581-3586.
21. Martín-de León, J., et al., Transparent nanocellular PMMA: Characterization and modeling of the optical properties. Polymer, 2019. **170**: p. 16-23.
22. Costeux, S. and L. Zhu, Low density thermoplastic nanofoams nucleated by nanoparticles. Polymer, 2013. **54**(11): p. 2785-2795.
23. Liu, S., et al., Bubble Seeding Nanocavities: Multiple Polymer Foam Cell Nucleation by Polydimethylsiloxane-Grafted Designer Silica Nanoparticles. ACS Nano, 2020. **14**(2): p. 1623-1634.
24. Toshiyuki Nomura, Manuel Alonso, Yasuo Kousaka, and Ken Tanaka, A Model for Simultaneous Homogeneous and Heterogeneous Nucleation. Journal of Colloid and Interface Science, 1998. **203**: p. 170–176.
25. Yeh, S.-K., et al., Effect of molecular weight to the structure of nanocellular foams: Phase separation approach. Polymer, 2020. **191**: p. 122275.
26. Martín-de León, J., V. Bernardo, and M. Rodríguez-Pérez, Low Density Nanocellular Polymers Based on PMMA Produced by Gas Dissolution Foaming: Fabrication and Cellular Structure Characterization. Polymers, 2016. **8**(7): p. 265.
27. Aher, B., N.M. Olson, and V. Kumar, Production of bulk solid-state PEI nanofoams using supercritical CO2. Journal of Materials Research, 2013. **28**(17): p. 2366-2373.